Article

Preliminary Beneficiation Studies of Quartz Samples from the Northwest Territories, Canada

Hanyu Zhang [1], Gideon Lambiv Dzemua [2] and Qi Liu [1,*]

[1] Department of Chemical and Materials Engineering, University of Alberta, Edmonton, AB T6G 1H9, Canada; hanyu7@ualberta.ca

[2] Northwest Territories Geological Survey, Yellowknife, NT X1A 2L9, Canada; gideon_lambiv@gov.nt.ca

* Correspondence: qi.liu@ualberta.ca

Abstract: Three quartz-rich geologic materials—vein quartz from the Great Bear Magmatic Zone, massive quartz from the Nechalacho rare earth deposit, and quartz sands from the Chedabucto silica sand deposit along the shores of the Northern Arm of the Great Slave Lake, Northwest Territories of Canada—were evaluated for their amenability to physical beneficiation into high-purity quartz (HPQ). The samples were subjected to various treatment processes, including crushing, grinding, calcining and quenching, acid leaching, wet high-intensity magnetic separation (WHIMS), and reverse flotation. After treatment, both the core and sand quartz samples met the requirements for HPQ, making them suitable for use in the production of semiconductor filters, liquid crystal displays (LCDs), and optical glass. However, the Al-bearing impurity content in the vein quartz products remained relatively high, and most of these impurities were dispersed in the quartz lattice, requiring further processing to meet the purity standards for HPQ required by these industries.

Keywords: vein quartz; core quartz; sand quartz; beneficiation; high-purity quartz; Northwest Territories

1. Introduction

Silicon (Si) is one of the most abundant elements in the Earth's crust, comprising about 27.7% of its mass, second only to oxygen which makes up 46.6% [1]. Quartz is the most common crystal form of silicon dioxide (SiO_2), accounting for 12.6% of the Earth's crust by volume [2]. Due to its robust physical and chemical properties, quartz has extensive applications in both traditional and high-tech industries [3]. It is widely used in refractory materials, mechanical casting, and chemical industry, among others [4]. Furthermore, quartz is widely used in high-tech industries because of its exceptional properties. For example, quartz is extensively used in fiber optical transmission and photovoltaic devices due to its high refractive index [5]. Its exceptional transparency allows it to be used in the production of quartz crystal glass, known as the "crown of glass materials" [4]. However, the presence of impurities, such as Fe and Al, reduces its light transmittance, affecting the performance of quartz glass and quartz optical fibers [6]. Purity is therefore an essential factor in determining the applications of quartz. Production of high-quality optical devices, semi-conductors, synthetic quartz wafers, and crucibles for solar-grade Si production, among others, requires high-purity quartz (HPQ) [4]. In the production of quartz crucibles used to hold high-temperature Si melts, impurities can make the crucibles opaque and cause brown spots on the surface of the produced Si crystals [7]. Generally, quartz with a SiO_2 content of 99.9% (3N) [8] is referred to as HPQ, while ultra-high-purity quartz (ultra-HPQ) has a SiO_2 content exceeding 99.998% (4N8) [9].

The demand for HPQ is increasing steadily because of the rapid development of the semiconductor and photovoltaic industries. Currently, there are two main methods to produce HPQ: artificial synthesis [10,11] or purification of natural quartz mineral. Artificial synthesis relies on high-purity starter crystals and uses vapor deposition with CCl_4 or

sol–gel methods [11]. Due to the high costs of synthesis and the depletion of high-purity starter crystal resources, there is a growing focus on producing HPQ and ultra-HPQ by purifying the more abundant natural quartz minerals [3,12]. Natural quartz minerals often contain various inclusions and lattice impurities, which are incorporated into the quartz during crystallization by processes like alteration, irradiation, diagenesis, or metamorphism under varying temperatures, pressure, and humidity. These may include point defects, dislocations, planar defects, and melt/fluid or mineral micro-inclusions [2]. To obtain HPQ, these impurities must be removed through appropriate treatment methods. Key quartz purification techniques include physical, chemical, and biological methods [13,14]. The physical and chemical methods can be further subdivided into processes such as grinding, screening, microwave heating, calcining and quenching, magnetic separation, flotation, acid leaching, ultrasonic treatment, and chlorination roasting [15–24].

The beneficiation of quartz requires grinding to liberate quartz from mineral impurities. Fine grinding is an energy-intensive process; thus, a proper grind size needs to be established to balance mineral impurity liberation and energy consumption [15]. Fluid inclusions are often present in quartz. Calcining followed by quenching is a common method for breaking fluid inclusions and removing associated impurities. Notably, the smaller the grain size of inclusions, the more challenging it is to remove them [25]. Microwave heating offers a novel approach for treating fluid inclusions. Unlike conventional calcination, microwave heating provides internal selective heating and is especially efficient for polar substances like water, which are susceptible to microwave treatment [16]. Magnetic separation and froth flotation are also effective methods for quartz beneficiation. Magnetic separation can remove even weakly magnetic mineral impurities from quartz using a strong magnetic field, while froth flotation achieves separation by exploiting differences in hydrophobicity between quartz and mineral impurities, through the use of flotation reagents to modify surface hydrophobicity [4,17]. Selective flocculation [26] and two-stage flotation [27] have been investigated in recent studies to enhance quartz flotation efficacy. The above physical ore dressing methods can enrich quartz to a high purity. For further beneficiation, chemical methods, such as acid leaching and chlorination roasting, may be applied. Acid leaching is a chemical reaction at the solid–liquid interface, where impurities dissolve into the slurry and are subsequently removed through solid–liquid separation. Common acids used in leaching to purify quartz include HCl, H_2SO_4, and so on. HF may also be used in some cases to achieve more pronounced upgrading effects, but it reacts with SiO_2, leading to a decrease in quartz yield [4,18]. Chlorination roasting is a method for ultra-HPQ production, whereby roasting alters the quartz crystal structure and disrupts impurity structures, and chlorine gas can volatize impurity elements from the quartz surface, facilitating their removal [28].

The Northwest Territories of Canada have many quartz-rich deposits, some with natural high quality. These include the giant quartz veins in the Great Bear Magmatic Zone (GBMZ), the massive quartz of the Quartz Core Zone (QCZ) in the Nechalacho rare earth mine, and the Chedabucto quartz sands along the shores of the Northern Arm of the Great Slave Lake. Byron [29] characterized the giant quartz veins at different zones in the GBMZ using electron microprobe analysis, scanning electron microscopy, X-ray diffraction, cathodoluminescence, and other methods. She found that although some of the zones hosted base metal and U mineralization, most were barren and only contained giant quartz veins. The quartz contained abundant fluid inclusions and some complex growth zones where Si was substituted by Al and Li. Quartz from the QCZ in Nechalacho contains very low concentrations of impurities, most of which were at the ppm level, including some problematic elements such as P, U, and Th [30]. Only Na had elevated concentrations at more than 100 ppm, which was predominantly observed in fluid inclusions. Hu [31] conducted a QEMSCAN mineralogical investigation of the −850 + 105 μm size fraction of quartz sand samples from Chedabucto sand. The primary mineral identified was quartz, with purity levels ranging from 95.88% to 99.54% SiO_2. Key impurities included orthoclase, Na-Ca feldspar, pyrite/marcasite, calcite/aragonite, kaolinite, and illite. The average

particle size of the quartz grains ranged from 150 to 236 µm, and impure mineral grains were generally smaller than 100 µm. QEMSCAN images showed that most quartz particles were pure and liberated, though some had intergrown impurities, mainly at the rim or in cracks, which may be removed by fine grinding and/or acid leaching. A very small number of particles had encapsulated impurities. The objective of this study was to upgrade samples from the above deposits to HPQ using simple and practical beneficiation methods.

2. Materials and Methods

2.1. Materials

Ten quartz samples from the Northwest Territories, Canada, were used in this study. These included three samples from a giant quartz vein in the GBMZ (labelled as S1, S2, and S3), four from the QCZ in the Nechalacho rare earth mine (S4, S5, S6, and S7), and three from the Chedabucto silica sand deposit along shores of the Northern Arm of the Great Slave Lake (S8, S9, and S10). Figure 1 shows photographs of the representative samples. As can be seen, the vein quartz samples showed irregular, blocky structures with noticeable surface textures. The samples were dense, primarily composed of translucent white to milky-white quartz interspersed with brown and grey coloration. The color variations were likely caused by lichens and mineral impurities. The surfaces exhibited some rough, uneven patches and occasional small cracks. The samples displayed a generally coarse grain size with vitreous luster in the milky-white area, suggesting their formation from HPQ materials. The samples from QCZ were HQ cores with a diameter of approximately 63.5 mm. The quartz appeared massive. The samples were translucent white to pale grey, with some fracture surfaces coated with reddish-brown iron oxide stains. Samples of the quartz sand were unconsolidated and appeared grey/brownish with particles generally measuring less than 500 µm. All quartz samples appeared to have high purity.

| (a) | (b) | (c) |
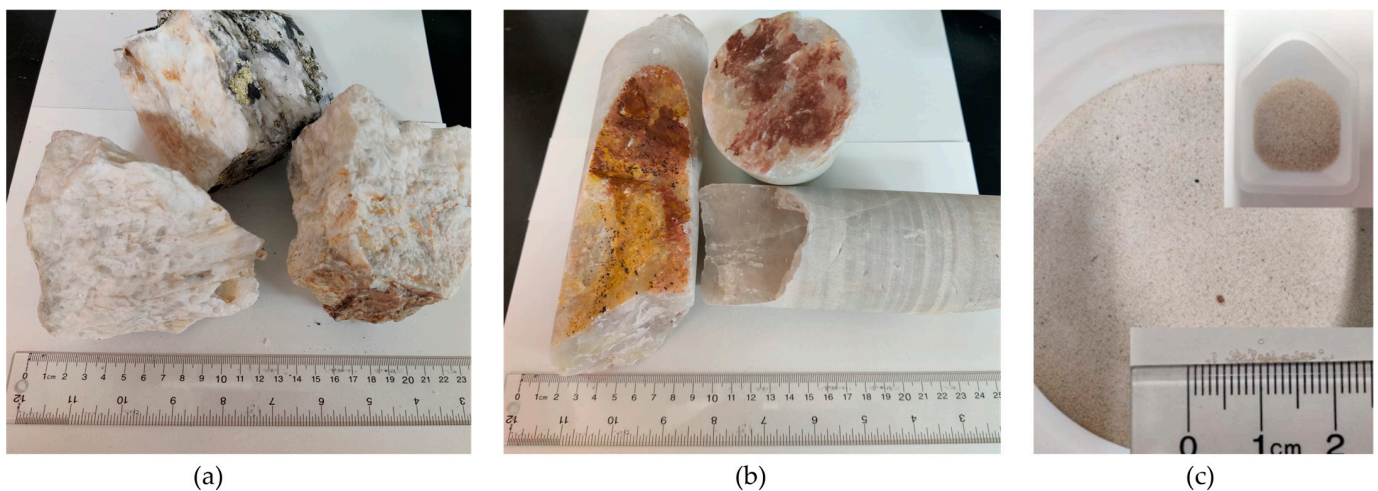
Figure 1. Photographs of quartz samples. (**a**) vein, (**b**) core, and (**c**) sand.

The particle size distribution of the three quartz sand samples was determined by sieve analysis. Figure 2 shows the cumulative particle size distribution and the weight retained in different size fractions. As can be seen, sample S8 was considerably finer than samples S9 and S10. The approximate median sizes of the three samples were 320, 390, and 450 µm, respectively.

The mineralogical composition of the ten samples was determined by powder X-ray diffraction (XRD) using a Bruker D8 XRD platform at the nanoFAB—Fabrication and Characterization Facility, located at the University of Alberta, after crushing and grinding. The 2θ range was from 10° to 80° with a scan speed of 5 degrees per minute. The patterns for all the samples are shown in Figure 3. The XRD patterns of all the samples exhibit

distinct characteristic quartz peaks with no impurity peaks, indicating the naturally high purity of the samples.

Particle size range (μm)	Percentage (%)		
	S8	**S9**	**S10**
+500	10.5	22.2	28.9
500-400	14.4	25.2	37.5
400-300	31.1	35.4	26.6
300-200	33.7	15.8	6.1
-200	10.3	1.4	0.9
Total	100.0	100.0	100.0
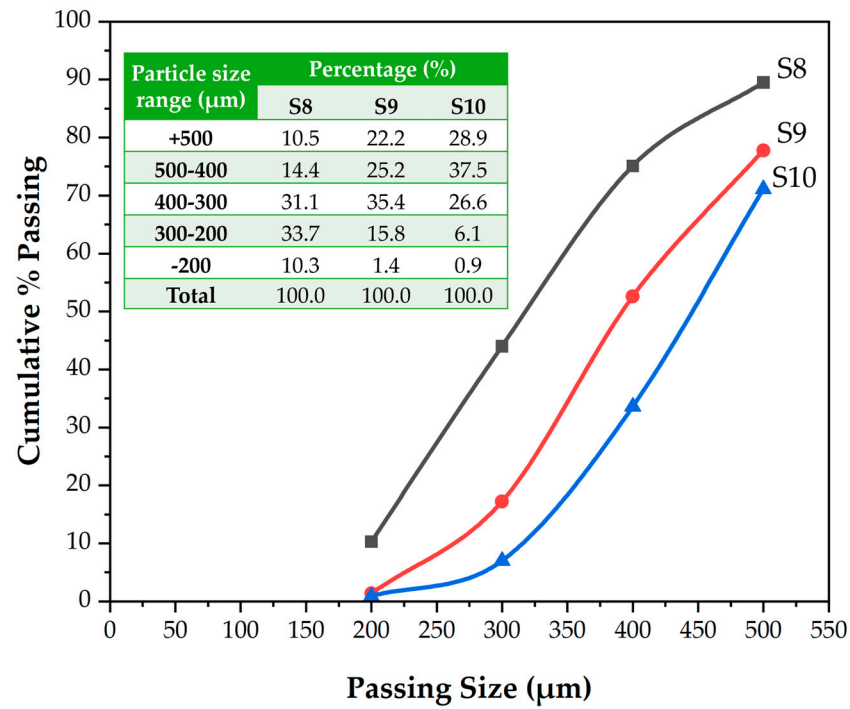
Figure 2. Cumulative particle size distribution of the three received quartz sand samples and particle size distribution table.
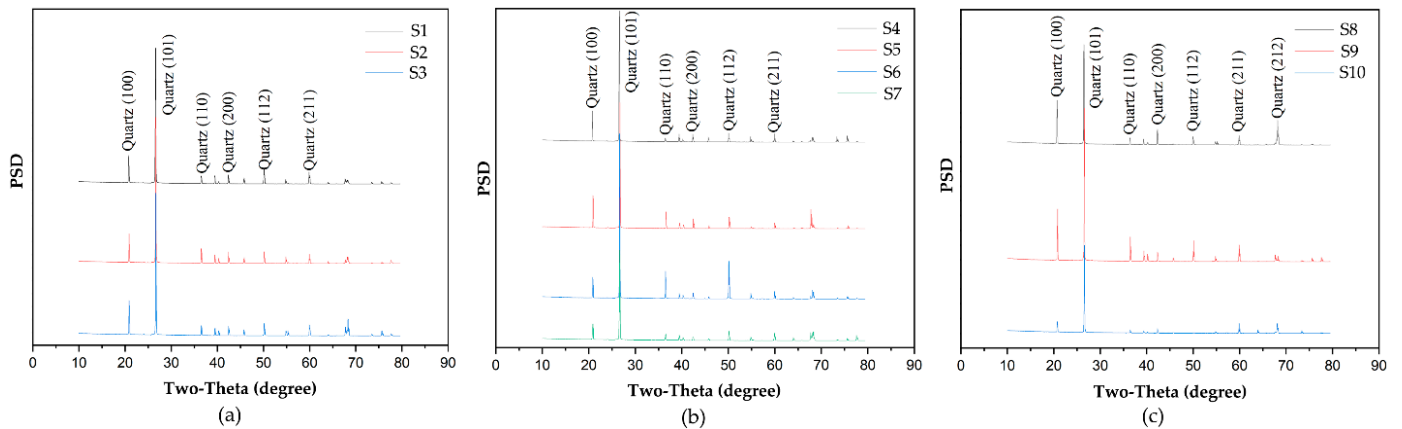
Figure 3. XRD patterns of quartz samples. (**a**) vein, (**b**) core, and (**c**) sands.

The chemical compositions of the samples were analyzed at the Geochem Laboratories of SGS Canada Inc. in Lakefield, Ontario. The SiO_2 content was directly measured by the gravimetric method according to ASTM C146, while the impurities were determined by whole-rock wavelength dispersion X-ray fluorescence (WD-XRF). The results are shown in Table 1. All ten samples had high SiO_2 content, ranging from 97.34% SiO_2 (Sample S1) to 99.19% (Sample S5). Vein and sand quartz samples had slightly lower purity, with Al and Fe being the main impurities. Therefore, removing Al and Fe should upgrade the SiO_2 purity.

Table 1. Composition of the ten quartz samples.

Sample	Composition (wt.%)							
	SiO$_2$	Al$_2$O$_3$	Fe$_2$O$_3$	MgO	CaO	Na$_2$O	K$_2$O	LOI
S1	97.34	0.73	0.14	0.05	0.06	0.09	0.12	0.55
S2	98.55	0.32	0.34	0.05	0.04	0.04	0.05	0.43
S3	98.35	0.33	0.35	0.06	0.03	0.02	0.06	0.49
S4	98.35	0.03	0.16	<0.01	0.02	0.03	<0.01	0.36
S5	99.19	<0.01	0.17	<0.01	0.02	0.03	<0.01	0.35
S6	98.63	0.02	0.3	0.04	0.02	0.04	<0.01	0.23
S7	98.06	0.02	0.42	0.06	0.21	0.03	<0.01	0.32
S8	97.79	0.18	0.03	<0.01	0.01	0.03	0.09	0.29
S9	98.03	0.27	0.06	<0.01	0.03	0.03	0.13	0.30
S10	98.02	0.25	0.05	<0.01	0.02	0.04	0.09	0.35

2.2. Beneficiation Processes

2.2.1. Reagents

Hydrochloric acid (HCl), sulfuric acid (H$_2$SO$_4$), oxalic acid (H$_2$C$_2$O$_4$), and sodium hydroxide (NaOH), all American Chemical Society (ACS) grade, were purchased from Fisher Scientific (Ottawa, Canada) and used for acid leaching and pH adjustment. Sodium oleate (active NaOl content ≥82%) was purchased from Millipore Sigma (Oakville, Canada) and used as a flotation collector. Dowfroth 250 (DF250) was acquired from Dow Chemical (Fort Saskatchewan, Canada) and used as a frother. Water used in all experiments was deionized (DI) water produced by Millipore Direct-Q® 5UV water purification system.

2.2.2. Experimental Procedures

Preliminary upgrading of quartz samples to HPQ is typically accomplished by conventional ore dressing techniques, including grinding, screening, magnetic separation, flotation, and acid leaching. More exotic treatment options could also be used for specific purposes, such as microwave heating or calcination followed by quenching to decrepitate fluid inclusions and expose their content, ultrasonic treatment to remove superficial contaminants, and chlorination roasting to volatize trace metals that are difficult to remove by physical ore dressing processes. The objective of this work was to enrich the SiO$_2$ content of the samples to 99.9% or higher using simple ore dressing techniques. Figure 4 illustrates the complete beneficiation process for the quartz samples used in this study, including size reduction, calcination and quenching, the first acid leaching using HCl, wet high-intensity magnetic separation (WHIMS), reverse flotation, and the second acid leaching using mixed H$_2$SO$_4$ and H$_2$C$_2$O$_4$.

Size reduction and pre-treatment: The vein quartz samples (S1, S2, and S3) and core samples (S4, S5, S6, and S7) were crushed with a Retsch BB 200 Jaw Crusher, followed by pulverization with a Retsch DM 200 Disc Pulverizer to minus 500 μm. The pulverized quartz samples likely had surface contamination from the crusher and pulverizer. Therefore, prior to subsequent beneficiation treatment, the pulverized <500 μm quartz samples were leached with 5% HCl at 60 °C at a liquid-to-solid ratio of 5:1. The leach slurry was agitated in a Corning LSE benchtop orbital shaker at 200 rpm for 8 h. The acid-leached samples were further ground using a Fritsch Pulverisette 2 mechanized agate mortar/pestle grinder to the required size (either 80% or 100% passing 50 μm, depending on the progression of the study). Since the sand quartz samples were <500 μm, no crushing was necessary. They were directly ground using an agate mortar/pestle grinder to either 80% passing 106 μm or 80% to 100% passing 50 μm, depending on the requirements of subsequent experiments.

Calcination and quenching: 10 g of each ground sample was calcined in a muffle furnace in which the temperature was ramped at 3.5 °C/min up to 800 °C and maintained for 2 h, and then immediately quenched in 1 L DI water. After quenching, the solids were separated from the liquid and 10 mL of the collected liquid was analyzed to determine

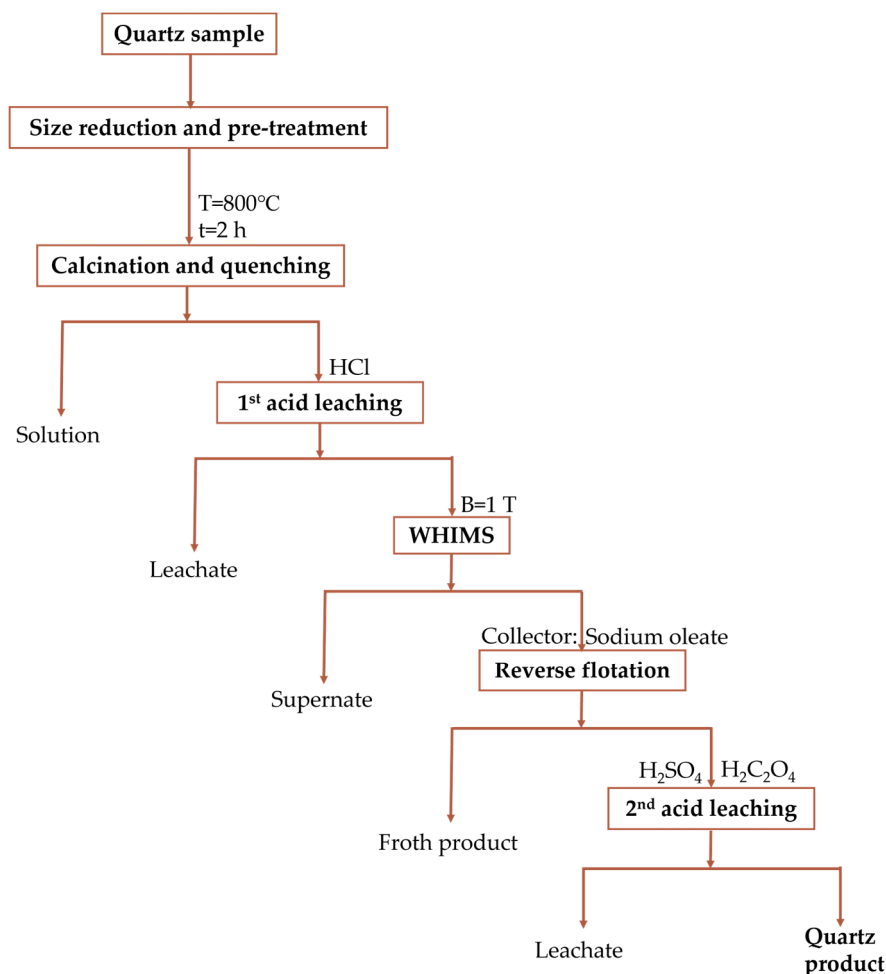its ionic composition. The solids (quartz samples) were dried and used for analysis and subsequent processing.

Figure 4. Flow chart of purification experiment.

Acid leaching: As shown in Figure 4, two steps of acid leaching were carried out. In the first step, a 10 g quartz sample was mixed with 10% HCl to create a slurry with a liquid-to-solid ratio of 10:1. The mixture was agitated using a Corning LSE benchtop orbital shaker at 200 rpm for 12 h at 60 °C. In the second acid leaching step, a 10 g quartz sample was leached with a mixture of 5% H_2SO_4 and 1% $H_2C_2O_4$, maintaining the same liquid-to-solid ratio of 10:1, at 70 °C and 200 rpm for 12 h. The experimental conditions mentioned above were determined through preliminary trials to achieve optimal efficiency, and the results of these trials are provided in Appendix A, Tables A1–A4. After each leaching step, 10 mL of the leachate was collected for chemical analysis, and the solids were filtered, washed, and dried for further analysis and processing.

WHIMS: Each sample was mixed with DI water to form a 20 wt.% solids slurry that was passed through the separation chamber of a WHIMS. The steel balls used in the chamber had a diameter of 10 mm, and the current was 5 A, i.e., enough to generate a strong magnetic field of approximately one Tesla. The samples that passed through the WHIMS while the current was turned on were the non-magnetic products. The current of the WHIMS was then turned off, and the retained solids in the separation chamber were flushed and rinsed to collect the magnetic product. Both streams of samples were collected and allowed to settle overnight and then decanted. Due to the high purity of the samples, the yield of the magnetic products was generally very low, in the 0.5–1% range.

Reverse flotation: Reverse flotation tests were performed in a 550 mm-tall and 50 mm-diameter flotation column, using 20 g of ground sample at 3 wt.% solids and at three different pH of 4, 5.6 (natural pH), and 10. Sodium oleate (NaOl) was used as a collector at dosages of 10, 100, 500, 1000, and 2000 g/t, with DF250 as the frother. The pulp was conditioned with NaOl for 5 min and floated for 1 min. The froth and tailing products were collected, filtered, and dried for analysis and further processing. The assay results of reverse flotation products under various conditions are provided in Appendix A, Tables A5–A8.

2.2.3. Analytical Methods

The compositions of liquid and solid samples were determined at the Geochem Laboratories of SGS Canada Inc., Lakefield, Ontario. The liquid samples were directly introduced into the inductively coupled plasma–optical emissions spectroscopy (ICP-OES) system to determine the concentrations of 30 elements, including Al, Fe, Na, and Ca. The SiO_2 content in the solid samples was measured directly by the gravimetric method according to ASTM C146. To measure the composition of impurities in the solid samples, the samples were fused with a lithium tetraborate/lithium metaborate mixture to form homogenous glass disks. The prepared disks were analyzed by WD-XRF, and the loss on ignition (LOI) was determined gravimetrically at 1000 °C using the G_PHY01V method (SGS Canada Inc.). We also used a benchtop Bruker CTX 801 X-ray fluorescence spectrometer to determine the compositions of interim quartz samples to guide the choice of upgrading methods and test conditions, and the results are reported in Appendix A. A Vega3 Tescan scanning electron microscope (SEM), equipped with energy-dispersive X-ray spectroscopy (EDS), and a Cameca SX 100 electron probe microanalyzer (EPMA) were used to analyze the form of Al impurities in the treated vein quartz samples, to determine whether they were present as discrete Al-bearing minerals or within the quartz lattice. The SEM-EDS was operated at an accelerating voltage of 20 kV, while the EPMA used an accelerating voltage of 15 kV, with a peak scan time of 60 s. The detection limit for Al was 12 ppm using the EPMA.

3. Result and Discussion

In this work, we did not apply all the processing steps described above to all ten quartz samples. Instead, the quartz sand sample S8 was used to scope the process conditions, and then one representative sample from each of the three sample groups was used to evaluate their responses to the conditions, and adjustments were made accordingly. Finally, all ten samples were processed using the established flowsheet.

3.1. Quartz Sand Sample S8

Sample S8 was selected for the scoping study because of its low SiO_2 content (97.8%). The sample was ground to 80% passing 106 μm, and then subjected sequentially to acid leach cleaning to remove superficial contaminants, calcining and quenching to remove fluid inclusions, HCl acid leaching, WHIMS, reverse flotation, and leaching by mixed H_2SO_4 and $H_2C_2O_4$. The change in SiO_2 content after each processing step is shown in Table 2.

As can be seen, acid leach cleaning increased the SiO_2 content of the sample from the original 97.79% to 99.13%. Subsequent processing steps, i.e., calcining and quenching, HCl leaching, and magnetic separation, increased the SiO_2 content to 99.67%, 99.68%, and 99.88%, respectively. However, reverse flotation did not lead to further enrichment, but rather resulted in a slight decrease in the SiO_2 content to 99.46%, indicating that further upgrading by reverse flotation was not possible. The second acid leaching using mixed H_2SO_4 and $H_2C_2O_4$ increased the SiO_2 content slightly to 99.64%.

The results of the various processing steps on Sample S8 showed that among the tested methods, acid leaching showed the best enrichment effect, followed by WHIMS. In contrast, the other methods showed limited effectiveness in enriching SiO_2 in the quartz sample. Regarding impurities, the most abundant contaminants were Al, Fe, K, and Na. While Fe

was removed almost completely after WHIMS, Al, K, and Na content remained unchanged. It is also worth noting that after reverse flotation, the quartz sample saw a slight increase in Na content, from 0.04% to 0.12%. This was likely caused by the addition of NaOl collector in the reverse flotation process.

Table 2. Assays of quartz sand sample S8 after sequential upgrading steps. SiO_2 content was determined directly by the gravimetric method according to ASTM C146, and impurity content was determined by whole-rock WD-XRF *.

Enrichment Process	Composition (wt.%)						
	SiO_2	Al_2O_3	Fe_2O_3	Na_2O	K_2O	P_2O_5	LOI
Original sample	97.79	0.18	0.03	0.03	0.09	0.02	0.29
Pre-acid leaching	99.13	0.17	0.04	0.04	0.09	0.01	0.29
Calcination & quench product	99.67	0.18	0.02	0.04	0.09	0.02	0.05
1st acid leaching product	99.68	0.15	0.03	0.05	0.08	<0.01	0.17
Non-magnetic product of WHIMS	99.88	0.12	<0.01	0.04	0.08	<0.01	0.08
Tailings from reverse flotation	99.46	0.16	<0.01	0.12	0.07	<0.01	0.23
2nd acid leaching product	99.64	0.17	<0.01	0.08	0.08	<0.01	0.26

* In addition to the components in this table, all the samples contain about 0.01% CaO and very little (<0.01%) of MnO, Cr_2O_3, and V_2O_5.

The solution obtained from calcining and quenching, and the leachates from the two acid leaching steps, were analyzed by ICP-OES, and the results are shown in Table 3. The concentration of ionic species in acid leach solutions is expected to be 10 times higher than that in the solution obtained after calcining and quenching because of the difference in the volumes of solution used. Therefore, the results of the quench solution should be multiplied by 10 for comparison purposes.

Table 3. Ionic composition of solution samples collected during the step-by-step processing of quartz sand sample S8.

Elements	Concentration (mg/L)			Elements	Concentration (mg/L)		
	Quench Solution	1st Acid Leaching Solution	2nd Leaching Solution		Quench Solution	1st Acid Leaching Solution	2nd Leaching Solution
Al	<0.2	17.5	2.8	Be	<0.003	<0.003	<0.003
Ba	<0.007	0.63	0.042	Bi	<1	<1	<1
Ca	3.3	5.1	5.6	Cd	<0.09	<0.09	<0.09
Cu	0.2	0.2	0.3	Co	<0.3	<0.3	<0.3
Fe	<0.2	8.1	2.3	Cr	<0.1	<0.1	<0.1
K	<1	5	1	Li	<2	<2	<2
Mg	0.45	1.86	2.32	Mo	<0.6	<0.6	<0.6
Mn	<0.04	0.09	0.36	Ni	<0.6	<0.6	<0.6
Na	8	7	15	P	<5	<5	<5
Pb	<2	3	<2	Sb	<1	<1	<1
Sr	0.054	2.86	0.039	Se	<3	<3	<3
Ti	<0.02	0.32	0.06	Sn	<2	<2	<2
Y	<0.02	0.07	<0.02	Tl	<3	<3	<3
Ag	<0.08	<0.08	<0.08	V	<0.2	<0.2	<0.2
As	<3	<3	<3	Zn	<0.7	<0.7	<0.7

As can be seen from Table 3, the quench solution showed relatively high concentrations of Ca, Mg, and Na, which were likely released from fluid inclusions in the quartz sand. The leachate from the first acid leaching (10% HCl) contained a relatively high concentration of Al (17.5 mg/L), along with significant amounts of Fe (8.1 mg/L), Na (7 mg/L), Ca (5.1 mg/L), Pb (3 mg/L), and Sr (2.86 mg/L). This indicates that HCl removed a considerable amount of impurities from the sample, especially Al. Subsequent acid leaching using a mixture of H_2SO_4 and $H_2C_2O_4$ removed a significant amount of Al (2.8 mg/L) and Fe (2.3 mg/L) but noticeably less than in the HCl leaching stage. However, the leach solution from the second-stage mixed acid leaching contained more Ca (5.6 mg/L), Cu (0.3 mg/L), Mg (2.32 mg/L), and Mn (0.36 mg/L) compared to the first acid leaching by HCl, suggesting that the combination of H_2SO_4 and $H_2C_2O_4$ had advantages in removing these multivalent metals compared to HCl.

3.2. Vein (S1), Core (S4), and Sand (S8) Samples

The sequential multi-step tests on sand quartz sample S8 showed that acid leaching had the most pronounced effect on enriching the SiO_2 content of the sample. Further leaching with mixed H_2SO_4 and $H_2C_2O_4$ removed additional impurities, especially multivalent metals, including Al and Fe. The other effective processing step was WHIMS, which was effective in removing Fe-bearing impurities. To simplify the process, one sample from each sample group—S1 from vein quartz, S4 from core quartz (S4), and S8 from sand quartz—was sequentially leached with mixed H_2SO_4 and $H_2C_2O_4$, and subjected to WHIMS. To enhance liberation and achieve better results, the samples were ground to 80% passing 50 μm.

Figure 5 shows SiO_2 content in the three samples, before and after acid leaching and magnetic separation. As can be seen, the SiO_2 content in the original samples was lowest in the vein sample (S1) at approximately 97.3% and highest in core sample (S4) at around 98.4%. The SiO_2 content in the sand sample (S8) was about 97.7%. After WHIMS, the SiO_2 content increased significantly, reaching approximately 99.1% in S1 and approximately 99.9% in S4 and S8. This demonstrated the effectiveness of grinding the samples to 80% passing 50 μm, followed by WHIMS. Subsequent leaching with a mixture of H_2SO_4 and $H_2C_2O_4$ further increased SiO_2 content. However, for the vein samples, grinding to 80% passing 50 μm was not effective in removing impurities further.
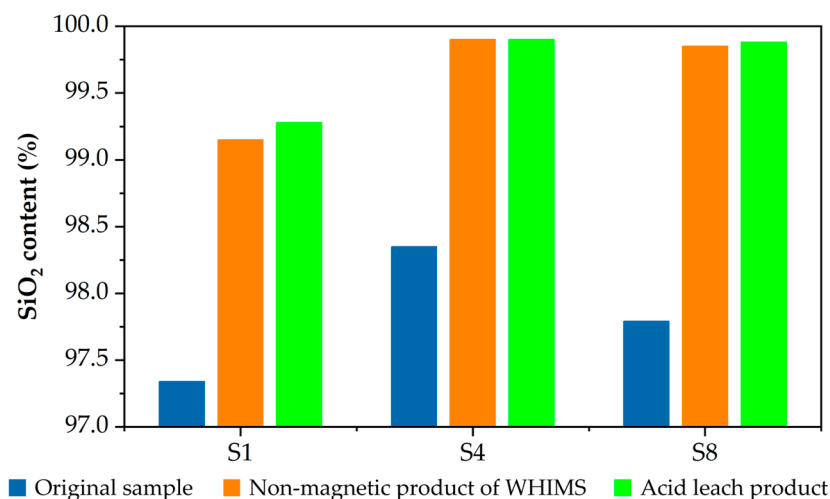

Figure 5. SiO_2 content, measured by the gravimetric method (ASTM C146) for S1, S4, and S8 after WHIMS and acid leaching with H_2SO_4 and $H_2C_2O_4$ mixtures.

3.3. Grinding, Magnetic Separation, and Acid Leaching of All Quartz Samples

Vein quartz samples were crushed and ground to 100% passing 50 μm, while the core quartz and sand samples were kept at 80% passing 50 μm. The beneficiation flowsheet relied on WHIMS followed by leaching with a mixture of H_2SO_4 and $H_2C_2O_4$.

As can be seen in Table 4, both WHIMS and acid leaching upgraded the SiO_2 content in all the quartz samples, with core quartz samples S4 and S5 showing the most significant improvement in SiO_2 content. The upgrade was lowest for the vein quartz samples, with SiO_2 content remaining below 99.9% even after reducing the particle size to 100% passing 50 μm. This indicated that magnetic separation and acid leaching are inefficient beneficiation methods for those vein quartz samples. The higher SiO_2 content of sample S1 after grinding to 100% passing 50 μm (99.49% SiO_2, Table 4) compared to the same sample ground to 80% passing 50 μm (99.28% SiO_2, Figure 5) indicates the effectiveness of particle size reduction in removing impurities and upgrading the SiO_2 content of vein quartz. The crushing/grinding step used in this study is easily achievable at an industrial scale, providing an efficient balance between impurity liberation and cost-effectiveness. Both WHIMS and acid leaching are standard processing techniques, widely recognized for their reliability and adaptability in large-scale production. Therefore, the approach developed here would be a feasible pathway for HPQ production from most of the tested quartz in an industrial setting.

Table 4. SiO_2 content of as-received quartz samples, as well as after magnetic separation and acid leaching. SiO_2 content was measured directly by the gravimetric method according to ASTM C146.

Sample	SiO₂ Content (wt.%)		
	Original Sample	Non-Magnetic Product	Acid Leach Product
S1	97.34	98.43	99.49
S2	98.55	98.76	99.05
S3	98.35	98.92	99.01
S4	98.35	>99.9	>99.9
S5	99.19	>99.9	>99.9
S6	98.63	99.65	99.76
S7	98.06	99.27	99.40
S8	97.79	99.85	99.88
S9	98.03	99.66	99.84
S10	98.02	99.79	99.86

Table 5 summarizes the SiO_2 content and major impurity content of each quartz sample after the beneficiation treatments (i.e., both magnetic separation and acid leaching. The data for the products of only magnetic separation is shown in Table A9). The vein quartz samples (S1, S2, and S3) were ground to 100% passing 50 μm, while the other seven quartz samples were ground to 80% passing 50 μm. As can be seen, after the complete beneficiation process, the vein quartz samples still contained a notable amount of Al_2O_3 impurities, ranging from 0.35% to 0.65%, while the concentrations of other impurities were negligible. In contrast, almost no impurities were detected in the core quartz samples, which showed the best beneficiation results. In addition, the sand quartz samples contained approximately 0.15% to 0.18% Al_2O_3, while other impurities were successfully eliminated.

Depending on the intended use, HPQ has different tolerance limits for Al and Fe impurities. For example, the Al_2O_3 and Fe_2O_3 content of HPQ used in the production of semiconductor filters, (LCDs), and optical glass (used in cameras, optical instruments, and optical fibers for telecommunications), should be below 2000 ppm (0.2%) and 100 ppm (0.01%), respectively [32]. In extremely high-end applications, such as large-size silicon wafers, the Al content is required to be less than 8 ppm [4]; in this case, the SiO_2 content should be at least 99.99%. Achieving such high purity goes beyond simple physical separation and is outside the scope of this work. It can be seen from Table 5 that samples of core and sand quartz met the basic quality requirements of HPQ after the grinding–

magnetic separation–acid leaching treatment. However, for the vein quartz samples, the Al content remained too high for HPQ standards, even after effectively controlling Fe-bearing impurities through magnetic separation. To meet HPQ requirements, additional processing will be needed to further lower the Al content of the vein quartz samples.

Table 5. Assay results for SiO_2 (gravimetric method according to ASTM C146) and the main impurities (whole-rock WD-XRF) of the ten quartz samples after grinding–magnetic separation–acid leaching treatments.

Sample	Composition (%)							
	SiO_2	Al_2O_3	Fe_2O_3	MgO	CaO	Na_2O	K_2O	P_2O_5
S1	99.49	0.65	0.01	0.04	<0.01	0.02	0.12	<0.01
S2	99.05	0.35	<0.01	0.03	<0.01	0.02	0.07	<0.01
S3	99.01	0.36	0.02	0.04	<0.01	0.02	0.08	<0.01
S4	>99.9	<0.01	<0.01	<0.01	<0.01	0.03	<0.01	<0.01
S5	>99.9	<0.01	0.01	<0.01	<0.01	0.01	<0.01	<0.01
S6	99.76	<0.01	0.01	<0.01	<0.01	0.01	<0.01	<0.01
S7	99.40	<0.01	0.05	<0.01	<0.01	0.02	<0.01	<0.01
S8	99.88	0.15	0.01	<0.01	<0.01	0.03	0.08	0.01
S9	99.84	0.17	0.01	<0.01	<0.01	0.03	0.08	0.02
S10	99.86	0.18	0.02	<0.01	<0.01	0.05	0.07	0.01

3.4. Aluminum-Bearing Impurities in the Vein Quartz Sample

Vein quartz sample S1 was selected for SEM-EDS and EPMA analyses. The particle size of the treated S1 sample was below 50 µm, allowing direct compaction for SEM-EDS analysis. Figure 6 shows the SEM scan results for an area of 1.38 mm × 1.38 mm at 200 times magnification. The sample is dominated by silicon and oxygen regardless of particle size, with only two Al-rich particles shown in the area: one in the upper left and one in the lower right (circled in red in Figure 6b). The map sum spectrum shows only a very small Al peak, with an integrated result indicating an Al content of 0.14 wt.%.

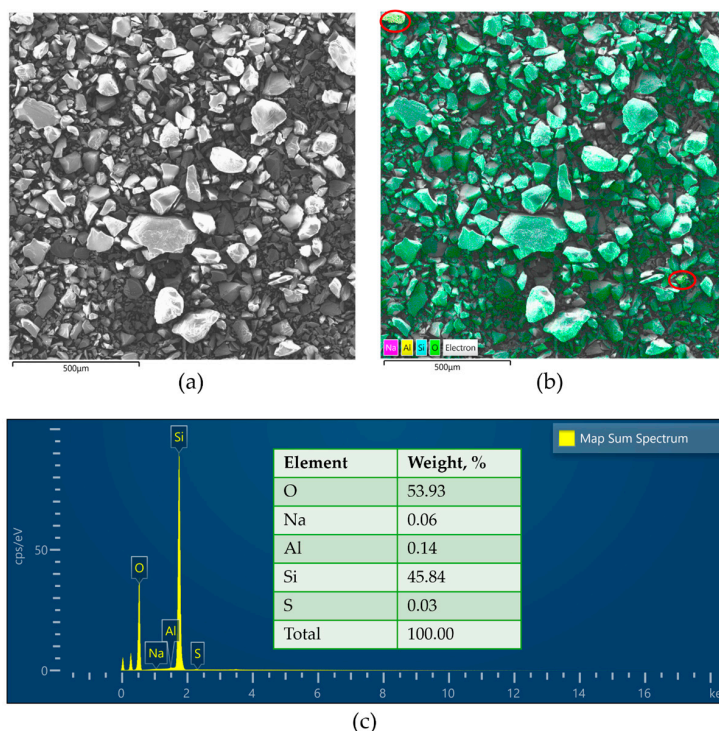| Element	Weight, %
O	53.93
Na	0.06
Al	0.14
Si	45.84
S	0.03
Total	100.00

Figure 6. SEM-EDS surface-scanning images of an area of the treated sample S1 (magnified 200 times). (**a**) Electron image, (**b**) EDS elemental distribution map (the particles indicated by red circles show enriched Al), and (**c**) map sum spectrum and the integral results of elemental content.

The composition of one of the Al-rich particles (Figure 7) was analyzed. The EDS spectrum indicates that the particle contains Si (28.42 wt.%), Al (11.77 wt.%), O (50.02 wt.%), Na (6.02 wt.%), and Ca (3.77 wt.%). Based on the above compositional data, the particle is likely a plagioclase feldspar. This indicates the presence of discrete Al-bearing mineral phases. The Al distribution map (Figure 7b) shows many scattered yellow dots, resembling background noise. This probably indicates Al dispersed within the quartz lattice. EMPA was then used to scan quartz-dominated regions in sample S1 to determine the amount of Al in the quartz lattice.
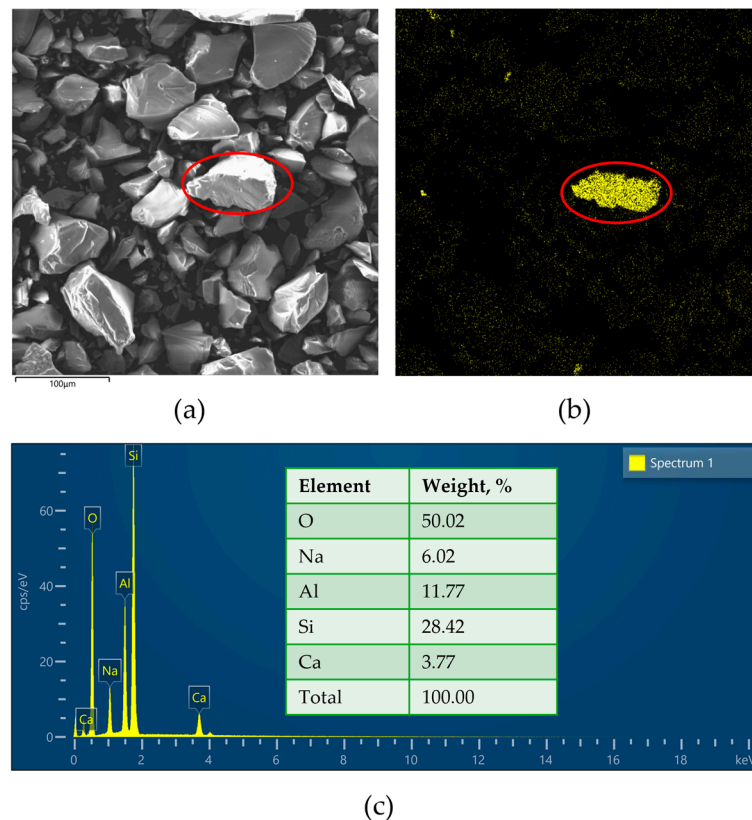

(a)   (b)

Element	Weight, %
O	50.02
Na	6.02
Al	11.77
Si	28.42
Ca	3.77
Total	100.00

(c)

Figure 7. SEM-EDS surface-scanning images of a selected small area of the treated sample S1 (magnified 700 times). (**a**) Electron image, (**b**) EDS Al distribution map, and (**c**) EDS compositional spectrum of the highlighted particle (indicated in the red circle).

To prepare samples for EPMA analysis, the quartz vein sample S1 should be embedded in epoxy and polished to expose a smooth surface suitable for scanning. Due to the small particle size of the treated samples (less than 50 µm), this polishing process could not be effectively applied. A piece of untreated S1 sample without visible impurity was polished to produce a surface on which about 100 randomly selected points with no visible impurities were analyzed for trace amounts of Al. The analyses detected Al in all 100 points, indicating that part of the Al in the quartz vein sample is incorporated within the SiO_2 lattice rather than solely as discrete mineral phases. Figure 8 shows the cumulative distribution function of Al content measured in S1 (the Al content for each point is shown in Table A10). The detected Al concentrations ranged from 229 ppm (0.0229 wt.%) to 4323 ppm (0.4323 wt.%). The cumulative distribution function curve shows a relatively gradual slope at the lower and higher ends, with a steeper slope near the median values, suggesting that most points cluster around the median (2566 ppm, or 0.2566 wt.%). The mean Al content across the 100 points was 2466 ppm (0.2466 wt.%), almost coinciding with the median. Combining this with the SEM-EDS results, it can be seen that discrete Al-bearing minerals amounted to about 0.14 wt.% Al (about 36% of total Al), and Al in quartz lattice amounted to around 0.25 wt.% Al (about 64% of total Al) of the compositions in the processed vein quartz

sample. While EPMA was performed on untreated samples, Al within the quartz lattice was likely not removed by WHIMS and acid leaching using H_2SO_4 and $H_2C_2O_4$. Therefore, the values can be used as proxies for the Al content in the processed sample. The Al content measured by SEM-EDS and EPMA adds up to about 0.39 wt.% of Al, corresponding to an Al_2O_3 content of 0.73 wt.%, close to the 0.65 wt.% Al_2O_3 determined by whole-rock WD-XRF analysis. About two-thirds of the Al impurities in the vein quartz sample are dispersed within the quartz lattice, and this type of impurity cannot be easily removed through traditional physical beneficiation methods. Remaining discrete Al impurities, in theory, could be removed by conventional ore dressing techniques. However, the reverse flotation experiments did not seem to remove the discrete Al-bearing minerals, likely due to insufficient liberation. Finer grinding may enhance the liberation and removal of the discrete Al mineral impurities. Excessive fine particles may, however, adversely impact flotation performance. Combined SEM-EDS and EPMA analyses suggest that even when the discrete Al-bearing minerals were removed, the SiO_2 content of the sample would still not reach 99.9%, because lattice Al contributed to about 0.25 wt.% Al, or 0.48 wt.% Al_2O_3. Indeed, our test work showed that all three vein quartz samples were upgraded to only 99–99.5 wt.% SiO_2, which could be considered the upper limit of physical ore dressing techniques for these vein quartz samples.
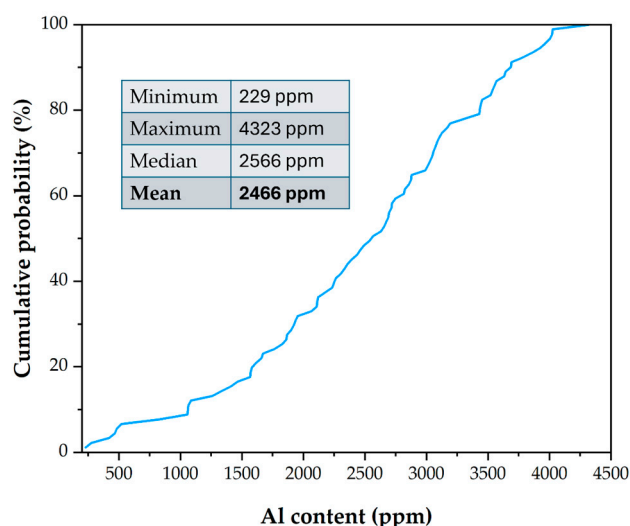

Figure 8. Cumulative distribution function of aluminum content measured at 100 points in quartz vein sample S1 using EPMA.

4. Summary and Conclusions

This work aimed to use simple and practical separation techniques for the preliminary beneficiation of ten quartz samples from the Northwest Territories, Canada. The samples included three samples from a giant quartz vein in the GBMZ, four from the QCZ in the Nechalacho rare earth mine, and three from the Chedabucto silica sand deposit along the shores of the Northern Arm of the Great Slave Lake. The separation techniques explored included grinding, calcining and quenching, acid leaching, WHIMS, and reverse flotation. The SiO_2 content in the original and treated samples was directly measured by the gravimetric method according to ASTM C146, and the contained impurities were determined by WD-XRF analysis. The impurities leached from the samples after calcining and quenching, and treatment with acids were analyzed by ICP-OES.

The initial SiO_2 content of the samples was already quite high at >97% SiO_2. WHIMS and acid leaching proved highly effective in increasing the SiO_2 content. In contrast, calcining and quenching, as well as reverse flotation, were less effective. A mixture of H_2SO_4 and $H_2C_2O_4$ acids was effective in removing impurities, especially for multivalent metals relative to hydrochloric acid (HCl) only. Combined grinding, WHIMS, and leaching with mixed acids H_2SO_4 and $H_2C_2O_4$ were effective in upgrading the SiO_2 content of the

samples. The Al_2O_3 content in all four core quartz samples after beneficiation was reduced to less than 100 ppm (0.01%), and the value for the three sand quartz samples was from 1500 to 1800 ppm (0.15%–0.18%). This meets the <2000 ppm (0.2%) requirement for the production of semiconductors, (LCDs), optical glasses, optical instruments, and optic fibers for telecommunications.

Using the developed process, the SiO_2 content in the vein quartz samples increased to 99.5%, slightly less than the 99.9% SiO_2 standard. While Fe_2O_3 content was low at 100–200 ppm (0.01%–0.02%) after the upgrading treatment, likely due to the high-intensity magnetic separation, the Al_2O_3 content remained high, between 0.35% and 0.65% (3500 ppm to 6500 ppm). SEM-EDS and EPMA analyses showed that, in the vein quartz sample S1, discrete Al-bearing minerals (plagioclase group minerals) contributed 0.14 wt.% Al (0.26 wt.% Al_2O_3), and lattice Al substitution of Si contributed about 0.25 wt.% Al (0.47 wt.% Al_2O_3), accounting for 0.73 wt.% Al_2O_3 in sample S1. The 0.47 wt.% Al_2O_3 in the quartz crystal lattice in the vein quartz sample S1 represents the limit of physical ore dressing techniques. Therefore, this vein quartz sample could not be physically upgraded to more than 99.53% SiO_2.

Author Contributions: Conceptualization, G.L.D. and Q.L.; methodology, H.Z., G.L.D. and Q.L.; formal analysis, H.Z. and Q.L.; investigation, H.Z. and Q.L.; resources, G.L.D. and Q.L.; writing—original draft preparation, H.Z.; writing—review and editing, G.L.D. and Q.L.; visualization, H.Z.; supervision, Q.L.; project administration, G.L.D. and Q.L.; funding acquisition, G.L.D. and Q.L. All authors have read and agreed to the published version of the manuscript.

Data Availability Statement: Data will be made available upon reasonable request.

Conflicts of Interest: The authors declare no conflicts of interest.

Appendix A

Table A1. SiO_2 content (%) of S1 (vein quartz), S4 (core quartz), and S8 (sand quartz) leached with HCl at 60 °C for 8 h under various HCl concentrations (5% or 10%) and liquid-to-solid ratios (5:1 or 10:1), measured by a Bruker CTX XRF spectrometer.

Sample	5% HCl Liquid/Solid = 5	10% HCl Liquid/Solid = 5	5% HCl Liquid/Solid = 10
S1	98.37	98.66	98.87
S4	98.94	99.01	98.97
S8	98.53	98.58	98.67

Table A2. Major composition of the acid leaching products for samples S1, S4, and S8, treated with HCl at varying concentrations (5% or 10%) and liquid-to-solid ratios (5:1 or 10:1) at 60 °C for 8 h, measured by a Bruker CTX XRF spectrometer.

Conditions	Composition (wt.%)							
	SiO_2	Al_2O_3	Fe	MgO	Ca	Mn	K_2O	Ti
S1, 5% HCl, Liquid/solid = 5	98.37	0.46	0.05	<0.01	<LOD	<0.01	0.07	<LOD
S1, 10% HCl, Liquid/solid = 5	98.66	0.64	0.05	<0.01	<LOD	<0.01	0.06	<LOD
S1, 5% HCl, Liquid/solid = 10	98.87	0.60	0.05	<0.01	0.01	<0.01	0.06	<LOD

Table A2. *Cont.*

Conditions	Composition (wt.%)							
	SiO$_2$	Al$_2$O$_3$	Fe	MgO	Ca	Mn	K$_2$O	Ti
S4, 5% HCl, Liquid/solid = 5	98.94	<LOD	<0.01	<0.01	<LOD	<0.01	0.02	<LOD
S4, 10% HCl, Liquid/solid = 5	99.01	<LOD	0.02	<0.01	0.01	0.01	0.02	<LOD
S4, 5% HCl, Liquid/solid = 10	98.97	<LOD	0.01	<0.01	<LOD	0.01	0.02	<LOD
S8, 5% HCl, Liquid/solid = 5	98.53	0.13	0.07	0.01	0.01	<LOD	0.07	<0.01
S8, 10% HCl, Liquid/solid = 5	98.58	0.11	0.07	<0.01	0.01	<LOD	0.05	<0.01
S8, 5% HCl, Liquid/solid = 10	98.67	0.09	0.07	<0.01	<LOD	<LOD	0.08	0.02

Table A3. SiO$_2$ content (%) in sample S8 after acid leaching under different conditions, measured by a Bruker CTX XRF spectrometer. The tests were conducted using H$_2$SO$_4$, H$_2$C$_2$O$_4$, HCl + H$_2$C$_2$O$_4$, and H$_2$SO$_4$ + H$_2$C$_2$O$_4$, at acid concentrations of 10% HCl, 5% H$_2$SO$_4$, and 1% H$_2$C$_2$O$_4$. The liquid-to-solid ratio was maintained at 10:1, with a stirring speed of 200 rpm.

Conditions	H$_2$SO$_4$	H$_2$C$_2$O$_4$	HCl + OA	H$_2$SO$_4$ + H$_2$C$_2$O$_4$
60 °C, 8 h	98.12	97.79	98.06	97.95
70 °C, 8 h	97.89	98.19	97.76	98.48
60 °C, 12 h	98.25	98.09	98.32	98.31

Table A4. Major composition measured by a Bruker CTX XRF spectrometer of the acid leaching products for sample S8 after acid leaching with various acids under different conditions. The tests were conducted using H$_2$SO$_4$, H$_2$C$_2$O$_4$, HCl + H$_2$C$_2$O$_4$, and H$_2$SO$_4$ + H$_2$C$_2$O$_4$, at acid concentrations of 10% HCl, 5% H$_2$SO$_4$, and 1% H$_2$C$_2$O$_4$. The liquid-to-solid ratio was maintained at 10:1, with a stirring speed of 200 rpm.

Conditions	Composition (wt.%)							
	SiO$_2$	Al$_2$O$_3$	Fe	MgO	Ca	Mn	K$_2$O	Ti
H$_2$SO$_4$, 60 °C, 8 h	98.12	0.09	0.07	<0.01	0.01	<LOD	0.08	<0.01
H$_2$SO$_4$, 70 °C, 8 h	97.89	0.10	0.07	<0.01	<LOD	<LOD	0.09	0.02
H$_2$SO$_4$, 60 °C, 12 h	98.25	0.10	0.07	<0.01	0.01	<LOD	0.08	0.01
H$_2$C$_2$O$_4$, 60 °C, 8 h	97.79	0.11	0.07	<0.01	0.01	<LOD	0.08	0.01
H$_2$C$_2$O$_4$, 70 °C, 8 h	98.19	0.11	0.07	<0.01	<LOD	<LOD	0.14	0.02
H$_2$C$_2$O$_4$, 60 °C, 12 h	98.09	0.08	0.07	<0.01	<LOD	<0.01	0.10	0.01
HCl + H$_2$C$_2$O$_4$, 60 °C, 8 h	98.06	0.07	0.07	<0.01	<LOD	<LOD	0.09	<0.01
HCl + H$_2$C$_2$O$_4$, 70 °C, 8 h	97.76	0.07	0.06	<0.01	<LOD	<LOD	0.11	0.01
HCl + H$_2$C$_2$O$_4$, 60 °C, 12 h	98.32	0.07	0.06	<0.01	0.02	<LOD	0.12	0.02
H$_2$SO$_4$ + H$_2$C$_2$O$_4$, 60 °C, 8 h	97.95	0.08	0.07	<0.01	0.01	<0.01	0.10	0.02
H$_2$SO$_4$ + H$_2$C$_2$O$_4$, 70 °C, 8 h	98.48	0.10	0.07	<0.01	<LOD	<LOD	0.10	0.01
H$_2$SO$_4$ + H$_2$C$_2$O$_4$, 60 °C, 12 h	98.31	0.07	0.07	<0.01	<LOD	<0.01	0.09	0.01

Table A5. SiO$_2$ content (%) in froth products and slurry products of the flotation tests of S8, measured by a Bruker CTX XRF spectrometer, using 1000 g/t sodium oleate as a collector under different pH values.

pH Value	SiO$_2$ Content in Froth Product (%)	SiO$_2$ Content in Slurry Product (%)
pH = 4	98.40	98.12
pH = 6.5	98.24	98.73
pH = 10	98.19	98.21

Table A6. Major compositions of froth and slurry products from the reverse flotation test of sample S8, measured by a Bruker CTX XRF spectrometer, using 1000 g/t NaOl as the collector at different pH levels.

Conditions		Composition (wt.%)							
		SiO_2	Al_2O_3	Fe	MgO	Ca	Mn	K_2O	Ti
Froth Product	pH = 4	98.40	0.13	0.07	0.01	<LOD	<LOD	0.07	0.03
	pH = 6.5	98.24	0.11	0.07	<0.01	<LOD	<LOD	0.05	0.01
	pH = 10	98.19	0.09	0.07	0.01	<LOD	<LOD	0.08	0.02
Slurry Product	pH = 4	98.12	0.07	0.06	<0.01	0.01	<LOD	0.11	<0.01
	pH = 6.5	99.73	0.10	0.07	<0.01	0.02	<LOD	0.12	0.01
	pH = 10	98.21	0.08	0.07	<0.01	0.01	<LOD	0.10	0.02

Table A7. SiO_2 content (%) in froth products and slurry products of the flotation tests of S8, measured by a Bruker CTX XRF spectrometer, using different dosages of NaOl.

NaOl Amount (g/t)	SiO_2 Content in Froth Product (%)	SiO_2 Content in Slurry Product (%)
10	98.41	97.65
100	98.05	97.61
500	97.60	98.04
1000	98.24	98.73
2000	98.29	98.18

Table A8. Major compositions of froth and slurry products from the reverse flotation test of sample S8, measured by a Bruker CTX XRF spectrometer, at varying NaOl collector dosages.

NaOl Amount (g/t)		Composition (wt.%)							
		SiO_2	Al_2O_3	Fe	MgO	Ca	Mn	K_2O	Ti
Froth Product	10	98.41	0.09	0.05	<0.01	0.02	<LOD	0.14	0.01
	100	98.05	0.13	0.05	<0.01	0.01	<0.01	0.14	0.01
	500	97.60	0.11	0.07	<0.01	<LOD	<LOD	0.10	0.02
	1000	98.24	0.10	0.07	<0.01	0.01	<LOD	0.12	0.03
	2000	98.29	0.11	0.06	<0.01	0.01	<LOD	0.09	0.01
Slurry Product	10	97.65	0.11	0.07	<0.01	0.01	<0.01	0.10	0.01
	100	97.61	0.10	0.06	<0.01	0.01	<LOD	0.11	0.02
	500	98.04	0.09	0.07	<0.01	<LOD	<LOD	0.12	0.01
	1000	98.73	0.08	0.06	<0.01	<LOD	<LOD	0.06	0.01
	2000	98.18	0.11	0.06	<0.01	<LOD	<LOD	0.06	0.01

Table A9. Major compositions of non-magnetic products of all the quartz samples, among which SiO_2 content, which was measured directly by the gravimetric method according to ASTM C146, while impurity content was determined by whole-rock WD-XRF.

Sample	Composition (%)							
	SiO_2	Al_2O_3	Fe_2O_3	MgO	CaO	Na_2O	K_2O	P_2O_5
S1	98.43	0.71	0.04	0.07	0.02	0.02	0.12	0.01
S2	98.76	0.39	0.08	0.06	0.02	0.01	0.08	<0.01
S3	98.92	0.39	0.14	0.07	<0.01	<0.01	0.08	<0.01
S4	>99.9	0.01	<0.01	<0.01	<0.01	0.02	<0.01	<0.01
S5	>99.9	0.05	0.02	<0.01	0.01	0.02	<0.01	<0.01
S6	99.65	<0.01	0.04	0.02	0.04	0.01	<0.01	<0.01
S7	99.27	<0.01	0.11	0.02	0.20	0.02	<0.01	<0.01
S8	99.88	0.15	0.01	<0.01	<0.01	0.03	0.09	<0.01
S9	99.66	0.24	0.03	0.01	0.02	0.05	0.10	0.02
S10	99.79	0.20	0.02	<0.01	0.02	0.05	0.07	0.02

Table A10. Data on the Al content at each point of the vein quartz sample S1 measured by EPMA.

Number	Al (wt.%)	Al (ppm)
1	0.3168	3168
2	0.2108	2108
3	0.2537	2537
4	0.2817	2817
5	0.2334	2334
6	0.3453	3453
7	0.3312	3312
8	0.3554	3554
9	0.4023	4023
10	0.4025	4025
11	0.1614	1614
12	0.2673	2673
13	0.3569	3569
14	0.2390	2390
15	0.2629	2629
16	0.2720	2720
17	0.2691	2691
18	0.2492	2492
19	0.3780	3780
20	0.1058	1058
21	0.1087	1087
22	0.2991	2991
23	0.1923	1923
24	0.2233	2233
25	0.2717	2717
26	0.1568	1568
27	0.2436	2436
28	0.0483	483
29	0.3644	3644
30	0.3430	3430
31	0.3073	3073
32	0.2879	2879
33	0.4323	4323
34	0.2248	2248
35	0.2462	2462
36	0.1828	1828
37	0.3087	3087
38	0.1954	1954
39	0.0229	229
40	0.2263	2263
41	0.3631	3631
42	0.3922	3922
43	0.1410	1410
44	0.2304	2304
45	0.4004	4004
46	0.3967	3967
47	0.3691	3691
48	0.3523	3523
49	0.2825	2825
50	0.1862	1862
51	0.3013	3013
52	0.3442	3442
53	0.1766	1766
54	0.2697	2697
55	0.1262	1262
56	0.1868	1868
57	0.1334	1334
58	0.2749	2749
59	0.3859	3859

Table A10. *Cont.*

Number	Al (wt.%)	Al (ppm)
60	0.3686	3686
61	0.3535	3535
62	0.2112	2112
63	0.3058	3058
64	0.2566	2566
65	0.1659	1659
66	0.2066	2066
67	0.1901	1901
68	0.3127	3127
69	0.3105	3105
70	0.2655	2655
71	0.2858	2858
72	0.3433	3433
73	0.2875	2875
74	0.3048	3048
75	0.1581	1581
76	0.1571	1571
77	0.2357	2357
78	0.3030	3030
79	0.2120	2120
80	0.3193	3193
81	0.0523	523
82	0.2175	2175
83	0.1466	1466
84	0.0277	277
85	0.1672	1672
86	0.0829	829
87	0.1065	1065
88	0.0467	467
89	0.1936	1936
90	0.1062	1062
91	0.0421	421

References

1. Konhauser, K.; Ehrlich, H.L.; Kappler, A.; Newmann, D.K. Geomicrobial interactions with silicon. In *Ehrlich's Geomicrobiology*, 6th ed.; CRC Press, Taylor & Frances Group: Boca Raton, FL, USA, 2016; pp. 237–255.
2. Götze, J. Chemistry, textures and physical properties of quartz—Geological interpretation and technical application. *Mineral. Mag.* **2009**, *73*, 645–671. [CrossRef]
3. Xia, M.; Yang, X.; Hou, Z. Preparation of High-Purity Quartz Sand by Vein Quartz Purification and Characteristics: A Case Study of Pakistan Vein Quartz. *Minerals* **2024**, *14*, 727. [CrossRef]
4. Pan, X.; Li, S.; Li, Y.; Guo, P.; Zhao, X.; Cai, Y. Resource, characteristic, purification and application of quartz: A review. *Miner. Eng.* **2022**, *183*, 107600. [CrossRef]
5. Braga, A.F.; Moreira, S.P.; Zampieri, P.R.; Bacchin, J.M.; Mei, P.R. New processes for the production of solar-grade polycrystalline silicon: A review. *Sol. Energy Mater. Sol. Cells* **2008**, *92*, 418–424. [CrossRef]
6. Islamov, A.K.; Ibragimova, E.; Nuritdinov, I. Radiation-optical characteristics of quartz glass and sapphire. *J. Nucl. Mater.* **2007**, *362*, 222–226. [CrossRef]
7. Yamahara, K.; Huang, X.; Sakai, S.; Utsunomiya, A.; Tsurita, Y.; Hoshikawa, K. Surface of silica glass reacting with silicon melt: Effect of raw materials for silica crucibles. *Jpn. J. Appl. Phys.* **2001**, *40*, 1178. [CrossRef]
8. Ling, W. Concept of high purity quartz and classification of its raw materials. *Conserv. Util. Miner. Resour.* **2022**, *42*, 55–63.
9. Zhang, R.; Tang, C.; Ni, W.; Yuan, J.; Zhou, Y.; Liu, X. Research Status and Challenges of High-Purity Quartz Processing Technology from a Mineralogical Perspective in China. *Minerals* **2023**, *13*, 1505. [CrossRef]
10. Khalifa, M.; Ouertani, R.; Hajji, M.; Ezzaouia, H. Innovative technology for the production of high-purity sand silica by thermal treatment and acid leaching process. *Hydrometallurgy* **2019**, *185*, 204–209. [CrossRef]
11. Moore, T.; Brady, B.; Martin, L.R. Measurements and modeling of SiCl4 combustion in a low-pressure H2/O2 flame. *Combust. Flame* **2006**, *146*, 407–418. [CrossRef]
12. Long, H.; Zhu, D.; Pan, J.; Li, S.; Yang, C.; Guo, Z. Advanced Processing Techniques and Impurity Management for High-Purity Quartz in Diverse Industrial Applications. *Minerals* **2024**, *14*, 571. [CrossRef]

13. Sarvamangala, H.; Natarajan, K. Microbially induced flotation of alumina, silica/calcite from haematite. *Int. J. Miner. Process.* **2011**, *99*, 70–77. [CrossRef]

14. Štyriaková, I.; Štyriak, I.; Kraus, I.; Hradil, D.; Grygar, T.; Bezdička, P. Biodestruction and deferritization of quartz sands by Bacillus species. *Miner. Eng.* **2003**, *16*, 709–713. [CrossRef]

15. Kohobhange, S.P.; Manoratne, C.H.; Pitawala, H.M.; Rajapakse, R.M. The effect of prolonged milling time on comminution of quartz. *Powder Technol.* **2018**, *330*, 266–274. [CrossRef]

16. Hou, Y.; Liu, P.; Hou, Q.; Duan, H.; Xie, Y. Study on removal fluid inclusions in quartz sand by microwave explosion. *Nanosci. Nanotechnol. Lett.* **2017**, *9*, 151–154. [CrossRef]

17. Yin, W.; Wang, D.; Drelich, J.W.; Yang, B.; Li, D.; Zhu, Z.; Yao, J. Reverse flotation separation of hematite from quartz assisted with magnetic seeding aggregation. *Miner. Eng.* **2019**, *139*, 105873. [CrossRef]

18. Zhang, Z.; Li, J.; Li, X.; Huang, H.; Zhou, L.; Xiong, T. High efficiency iron removal from quartz sand using phosphoric acid. *Int. J. Miner. Process.* **2012**, *114*, 30–34. [CrossRef]

19. Palaniandy, S.; Azizli, K.A.; Hussin, H.; Hashim, S.F. Study on mechanochemical effect of silica for short grinding period. *Int. J. Miner. Process.* **2007**, *82*, 195–202.

20. Buttress, A.J.; Rodriguez, J.M.; Ure, A.; Ferrari, R.S.; Dodds, C.; Kingman, S.W. Production of high purity silica by microfluidic-inclusion fracture using microwave pre-treatment. *Miner. Eng.* **2019**, *131*, 407–419.

21. Li, F.; Jiang, X.; Zuo, Q.; Li, J.; Ban, B.; Chen, J. Purification mechanism of quartz sand by combination of microwave heating and ultrasound assisted acid leaching treatment. *Silicon* **2021**, *13*, 531–541. [CrossRef]

22. Xiong, K.; Pei, Z.Y.; Zang, F.F.; Lin, M. Process and mechanism of high-purity quartz prepared by mixed acid leaching. *Non-Met. Mines* **2016**, *39*, 60–62.

23. Shaban, M.; AbuKhadra, M.R. Enhancing the technical qualifications of Egyptian white sand using acid leaching; response surface analysis and optimization. *Int. J. Miner. Process. Extr. Metall.* **2016**, *1*, 33–40.

24. Zhao, H.L.; Wang, D.X.; Cai, Y.X.; Zhang, F.C. Removal of iron from silica sand by surface cleaning using power ultrasound. *Miner. Eng.* **2007**, *20*, 816–818. [CrossRef]

25. Gaweł, B.A.; Ulvensøen, A.; Łukaszuk, K.; Muggerud, A.M.F.; Erbe, A. In situ high temperature spectroscopic study of liquid inclusions and hydroxyl groups in high purity natural quartz. *Miner. Eng.* **2021**, *174*, 107238. [CrossRef]

26. Mweene, L.; Khanal, G.P.; Kawala, J.; Chikontwe, K. Experimental and theoretical investigations into the surface chemical properties and separation of serpentine from quartz using xanthomonas campestris as a selective flocculant. *Miner. Eng.* **2024**, *217*, 108925. [CrossRef]

27. Silva, K.; Filippov, L.O.; Piçarra, A.; Flilippova, I.V.; Lima, N.; Skliar, A.; Faustino, L.; Leal, F.L. New perspectives in iron ore flotation: Use of collector reagents without depressants in reverse cationic flotation of quartz. *Miner. Eng.* **2021**, *170*, 107004. [CrossRef]

28. Guo, W.; Lu, H.; Zhang, Z.; Jiang, L.; Wu, H.; Liu, D.; Chi, R. Crystal structure transformation and lattice impurities migration of quartz during chlorine roasting. *Int. J. Min. Sci. Technol.* **2024**. [CrossRef]

29. Byron, S. Giant Quartz Vein Zones of the Great Bear Magmatic Zone, Northwest Territories, Canada. Master's Thesis, University of Alberta, Edmonton, AB, Canada, 2010; p. 146.

30. Steele-MacInnis, M.; Poulette, S. Report on Characterization of Quartz from Nechalacho. In *Final (Internal) Report to Northwest Territories Geological Survey*; 2022; p. 12.

31. Hu, P. QEMSCAN Mineralogy Investigation of 6 Frac Sand Sample Collected from "RC27654". In *Final (Internal) Report Prepared by AGAT Laboratories for Norwest Corporation*; 2017; p. 16.

32. Vatalis, K.I.; Charalambides, G.; Benetis, N.P. Market of high purity quartz innovative applications. *Procedia Econ. Financ.* **2015**, *24*, 734–742. [CrossRef]